General Disclaimer

One or more of the Following Statements may affect this Document

- This document has been reproduced from the best copy furnished by the organizational source. It is being released in the interest of making available as much information as possible.

- This document may contain data, which exceeds the sheet parameters. It was furnished in this condition by the organizational source and is the best copy available.

- This document may contain tone-on-tone or color graphs, charts and/or pictures, which have been reproduced in black and white.

- This document is paginated as submitted by the original source.

- Portions of this document are not fully legible due to the historical nature of some of the material. However, it is the best reproduction available from the original submission.

Final Report

to

THE NATIONAL AERONAUTICS AND SPACE ADMINISTRATION

for

NASA Contract NASW 3273

(NASA-CR-169190) SPACE ENVIRONMENT AND LUNAR SURFACE PROCESSES, 2 Final Report (CosmoScience Associates, Inc.) 53 p HC A04/MF A01 CSCL 03B

N82-30205

Unclas
G3/91 15146

SPACE ENVIRONMENT AND LUNAR SURFACE PROCESSES: II

Principal Investigator: Dr. George M. Comstock

COSMOSCIENCE ASSOCIATES, INC.

21 Erland Road, Stony Brook, N.Y. 11790

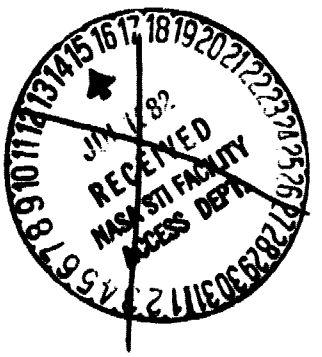

January 31, 1982

INTRODUCTION

It has long been recognized that the top few millimeters of a surface exposed to space represents a physically and chemically active zone with properties much different from those of a surface in the environment of a planetary atmosphere. It is in this zone that the material comprising the surface of the moon, Mercury, the asteroids, and similar bodies achieves physical and chemical maturity as a result of exposure to the solar wind (SW), solar flare (SF) particles, galactic cosmic rays (GCR), heating by solar radiation, and to the bombardment by meteoroids of a vast size range.

The recent work of several groups continues to clarify the nature of the processes involved at space-exposed surfaces. These include SW ion implantation and redistribution (Tamhane et al., 1979; Warhaut et al. 1979) and sputtering effects (see review paper by Pillinger, 1979), the origin and distribution of metal particles determining the ferromagnetic resonance (FMR) maturity index (Morris, 1980), shock effects and the formation of glass and agglutinates (Schaal and Hörz, 1980), and the effect of intergrain adhesive forces (Housley, 1980).

There has been a clear need for a quantitative synthesis of the various processes into a self-consistent picture of surface evolution. This synthesis is especially important as different experimental approaches have often resulted in apparently conflicting interpretations of soil history at specific sites. Recently Wieler et al. (1980) have attacked the problem experimentally by measuring noble gas concentrations in individual grains and comparing these with track distributions from the

same soil sample. This approach is very useful as it is often risky to correlate data measured on different samples.

The present work represents a step in our continuing effort to achieve a model synthesis. This study draws upon the experience gained from earlier models by the author and other groups (e.g., Gault et al., 1974; Arnold, 1975; Duraud et al., 1975; Borg et al., 1976; Comstock, 1977, 1978).

To obtain the results described here we developed a new set of computer programs called MESS.2 (Comstock, 1979, 1981). The design of the MESS.2 system is described in our Final Report for NASA Contract NAS 9-15582 submitted September 25, 1979. This current model differs from earlier work in that surface processes are broken down as a function of size scale and treated in three dimensions with good resolution on each scale. Since the smaller size scales are on the order of a grain diameter this approach derives explicitly the time and depth dependence of parameters as functions of grain size as well as of sample size, mixing depth, and surface layer residence time. Factors relevant to grain size dependence have been discussed by several authors (Fugster et al., 1975; Criswell, 1975; Becker, 1977; Bogard, 1977; Criswell and Basu, 1978; Housley, 1980).

Our results here apply to the development of soil residing near the surface for the first time and hence should describe immature to submature soils. The development of mature soils through further exposure and mixing can also be derived using these results. The current model is based on lunar conditions where considerable data exist to provide guidance and calibration. The model parameters can readily be adjusted to describe asteroid regoliths and other space-exposed bodies.

Grain redistribution.

MESS.2 breaks the surface soil down to a series of relevant size scales or regimes, simulates each regime separately and combines the results in an appropriate statistical manner. The structure of a given regime is shown schematically in figure 1. The depth scale is determined by the bottom of the model layer, depth D_L. A surface zone of depth D_Z is defined corresponding to the model layer of the next smaller size regime. Similarly D_L corresponds to the surface zone of the next larger size regime.

For a given regime a range of impact event sizes is simulated such that the largest events will generally just disrupt the full model layer depth, while the smallest events will generally just disrupt the surface zone. Hence the events occuring in larger size regimes will determine the local residence time for the model layer while events considered in the given regime control the local residence time of the surface zone. Events in the given regime also primarily control the ejection of material into the surface zone and subsequent reburial below it over a time scale comparable to the average residence time of the model layer. Details of the soil history within the surface zone are controlled by smaller size regimes. The events that effect a given regime will create a mixed zone of variable depth D_R which contains all material ejected by the simulated events.

Clearly this procedure only approximates the true behavior of the soil, we must emphasize that our purpose is not to

attempt to simulate the soil precisely but only to efficiently model the physically important processes governing its observed characteristics.

In the current work we use $D_Z = D_L/10$ for all regimes. In each regime the smallest crater simulated has a diameter equal to D_L, most events have a diameter less than about 3 D_L. Depths are monitored on a continuous scale while the surface is divided into an hexagonal grid, to enhance inherent circular symetries, of about 3000 cells where the cell diameter is no larger than D_Z. This assures good resolution for all events. The location of up to 12,000 individual particles of a given grain size is monitored by MESS.2. For about 200 of these we also monitor central track density and surface-zone residence time, initially these tagged grains are pristine and randomly distributed throughout the model layer.

For each grain size there will be a size regime such that the surface zone corresponds to a grain diameter and the smallest event will barely eject some grains intact. This is the smallest size regime modelled for a representative grain size, referred to as the base regime. In this regime the individual particles move in a matrix of order-of-magnetude finer material so as to approximate a typical size distribution. In this way the graininess of the soil and shielding of individual grains near the surface is taken into account in deriving distributions of exposure time and track density. A detailed size distribution of the matrix is not considered, so possible shielding by a thin layer of relatively very small particles is included only through a constant exposure factor (f) which is discussed in

detail later. In larger size regimes all grain sizes tend to behave alike, but smaller grains have smaller size base regimes and therefore generally experience a different dynamical history near the surface. This contributes to the overall grain size dependence of characteristics requiring surface exposure.

We are interested in grain sizes ranging from less than 10 microns to greater than 1 mm in diameter. Soil samples usually average over intervals ranging from 1 mm to 1 cm in soil columns to several centimeters in scoop samples. Therefore in this work we investigate the size regimes D_L = 100 microns (base regime for 10 micron grains), D_L = 1 mm (base regime for 100 micron grains), D_L = 1 cm (base regime for 1 mm particles), and D_L = 10 cm. The results will apply to soil which has resided once within 10 cm of the surface and should characterize immature to submature soils.

The motion of ejected material is followed in three dimensions during each impact event according to an ejecta origin model. The ejecta map we have developed for MESS.2 is shown in figure 2. The map was designed to be consistent with the results of Stöffler et al. (1975), one of the few experimental studies which clearly defines the ejecta origin for soil craters in the 10 cm diameter range. The work of Vedder (1972) suggests that the ejecta distribution for craters on the order of 100 microns diameter is probably much broader than that shown in figure 2. This will not be important to our results however since on this small scale our individual grains are deposited in essentially a single layer after ejection and hence their exact location is not statistically significant. For craters larger

than a few centimeters ejecta mapping and stratigraphy reversal occur in MESS.2 events.

Our submeter craters are based on the few experimental studies available (e.g., Braslau, 1970; Vedder, 1972; Stöffler et al., 1975; Gault and Wedekind, 1977). The work of Gault and Wedekind (1977) can be applied to the moon because they determine the dependence of crater parameters on gravitational acceleration. They find a crater depth H to rim diameter D_C ratio $H/D_C = 0.2$ for a 15 cm crater, essentially independent of gravity. Stöffler et al. (1975) obtain similar results but show further that the lower part of the crater is not ejected but compressed into the crater floor. Their craters in weak quartz sand show an ejected depth H_C to diameter ratio closer to $H_C/D_C = 0.1$; in more cohesive lunar soil the ratio may somewhat greater than this. Vedder (1972) investigated much smaller craters of about 100 micron diameter in a more cohesive test soil and obtained $H/D_C = 0.2 - 0.3$ much of which represented compressed material. We have adopted a value of $H_C/D_C = 0.15$ over the full size range studied and only material actually ejected is considered redistributed. MESS.2 ignores soil compression and density variations in general as second-order effects on the irradiation history of a grain. Depth scales in this paper apply for a soil density of 1.5 - 2.0 g/cm^3. We have taken local topography into account such that crater volume is maintained while generating a smooth crater that follows local slopes.

The size-frequency distribution of small soil craters cannot be determined by direct count as the lunar surface is

saturated with craters on this scale. Instead we use the size-frequency distribution of pits observed in rock surfaces and translate this to soil craters using the pit size to projectile mass relation and assumed velocity given by Hörz et al. (1975). For pit diameter DP in cm and projectile energy E in ergs their calibration yields $D_p = 2.1 \times 10^{-4} E^{0.37}$. The work of Gault and Wedekind (1977) would then indicate that a lunar soil crater of $D_C = 25$ cm would correspond to a 1 cm rock pit, or $D_C/D_P = 25$. However Gault and Wedekind used dry quartz sand to minimize strength effects so we should assume that 25 represents a maximum value for this ratio in the lunar case. Braslau (1970) obtained results similar to those of Gault and Wedekind. Vedder (1972) finds that soil craters are smaller in more cohesive soil indicating that strength effects are important in this size range. Gault and Wedekind reach a similar conclusion even in the case of dry quartz sand. The results of Vedder (1972), using a much lower projectile energy and a more cohesive soil indicate that a similar ratio $D_C/D_P = 10 - 20$ should be valid down to 100-micron diameter craters.

For the size-frequency distribution of impact pits we can combine the results of Hörz et al. (1974, 1975) and Morrison and Zinner (1977) to obtain an approximate analytic form:

(1) $$N(>D_C) = A\,(D_C/R_X)^{-3} + B\,(0.005 + D_C/R_X)^{-3}$$

where N is the cumulative pit production rate per cm^2-My, DC is in cm, $R_X = D_C/D_P$, and the constant 0.005 reflects a jog in the pit distribution at 10 - 100 microns. A is about B/1000 but the first term in equation 1 is not important for the redistribution of grains with diameters of about 10 microns or more.

Hörz et al. (1974) use $B = 8.3 \times 10^{-4}$, Comstock (1978) suggested that a value up to 10 times higher might be more consistent with track gradients in dusty rocks. Hörz et al. (1975) discuss sources of uncertainty in the long-term micrometeoroid flux.

Considering the uncertainties in D_C/D_P and in meteoroid flux we have defined a model time denoted MT such that 1 MT corresponds to 1 My (10^6 years) in the case of $D_C/D_P = 20$ and $B = 8.3 \times 10^{-4}$. The value of MT is inversely proportional to production rate N and, for $D_C \geq 1$ cm, inversely proportional to $(DC/DP)^3$, so the uncertainty in the time scale MT might be as much as an order of magnetude. However we show later that an assignment of 1 MT = 1 My is supported by calibrating the model results against lunar data. Note that the time scale depends on the cohesiveness of the soil through the ratio D_C/D_P.

Grain alteration.

In addition to the redistribution of soil particles as discussed above particles also experience the effects of irradiation, erosion, fragmentation, aggregation, and shock metamorphosis.

MESS.2 accumulates particle tracks continuously in the tagged grains using the solar flare track production rate given by Comstock (1978) of $7 \times 10^5 \, d^{-2.2}$ cm^{-2}-My^{-1} for depth d in g/cm^2 below a plane surface, and the galactic cosmic ray track rate given by Walker and Yuhas (1973) which predominates below about $d = 0.5$ g/cm^2 (about 3 mm of soil). In the base regime for a given grain size the central track density is accumulated at every depth the grain resides. In larger size regimes tracks

are accumulated only at depths below the surface zone and added to those accumulated in smaller regimes as a function of surface zone residence time. In this way the contribution from each level of residence is obtained explicitly.

The measured flux of solar wind ions is reviewed by Pillinger (1979). The observed concentration of implanted SW ions depends on retention characteristics different for each species and host mineral as well as surface exposure time. In this paper we derive only with exposure time and residence times within each depth zone. In the base regime MESS.2 monitors the actual surface exposure time of tagged grains. In larger regimes the time spent within the surface zone is monitored.

We are concerned here with processes which effect the irradiation record of an ensemble of grains over a time scale appropriate to a single residence episode within 10 cm of the surface. We are particularly concerned with effects important at the surface or varying with grain size. Among these are direct erosion of exposed grains and fragmentation of grains by direct impact. We find that these strongly effect the magnetude and grain size dependence of the irradiation record.

We assume that a grain of diameter D_G will be fragmented if it receives a direct impact generating a pit of diameter $D_P > D_G/8$. This value is uncertain and varies with condition of the grain, but smaller pits have been observed on soil grains while a pit approaching D_G must certainly fragment it. For the micrometeoroid flux used to obtain equation 1 with $B = 8.3 \times 10^{-4}$ this yields a lifetime T_1 against fragmentation for 10 micron, 100 micron, and 1 mm grains of about 3 My, 2 My, and 1 My, re-

spectively, with considerable uncertainty. With 10 times higher flux these become 0.3 My, 0.2 My, and 0.1 My, respectively. We have performed our calculations for both of these sets of values but since the shorter lifetimes have much more effect, for clarity we compare only the results for the shorter T_1 against the results assuming no fragmentation.

Fragmented grains are removed from their size population. Surface fragmentation will tend not to effect the low track density parameters such as the minimum and quartile since it will remove only those grains which have resided on the surface long enough to attain the highest densities. It can have a strong effect on solar wind concentration however since it removes those particles which have received the greatest SW fluence and hence control the total concentration.

The erosion of exposed grain surfaces by micrometeoroids too small to fragment the grain is generally not a significant process because of the low flux involved. The most important source of grain erosion relevant to SW ion implantation is atomic sputtering by solar ions (Pillinger, 1979; Flavill et al., 1980) who report a consensus of recent measurements suggesting a rate of 0.025 to 0.045 Å/year at the lunar equator. For a typical implantation depth of 300 Å (Pillinger, 1979) this leads to an implantation/erosion equilibrium on a time scale of T_s = 0.01 My. We present model calculations both with and without an effective SW saturation with this time constant.

This saturation time depends on implantation depth and so will vary with species (Pillinger, 1979). It has been suggested by Signer et al. (1977) that diffusional processes also leads

to a certain saturation time constant. Wieler et al. (1980) note that diffusion and sputter controlled saturation will have similar effects. Likewise the MESS.2 calculations depend only the time constant, whether this time constant arises from sputtering or diffusional processes is not readily determinable using our results.

The formation of agglutinates by shock compaction during micrometeoroid impact also occurs within the top millimeters. This process loads the agglutinate with irradiated grains and reduction metal. Thus residence time within the first few millimeters controls the noble gas and FMR characteristics of agglutinates. MESS.2 is designed to monitor glass and agglutinate production but these will not be discussed in detail here. Glass and agglutinate production and shock comminution throughout the soil volume become increasingly important as the soil matures and these processes must be taken into account explicitly in any simulations of mature soil.

MODEL RESULTS

Monte-Carlo calculations.

To illustrate the results produced by the MESS.? model we show in figures 3 - 14 some of the residence time and track density distributions derived for 100-micron diameter grains. Soil grains with diameter on the order of 100 microns are typically the more common sized particles in lunar soils. Similar distributions were also derived for representative particle diameters D_C = 10 microns and 1 mm. Figures 3 - 9 indicate distributions not yet including fragmentation loss. In figures 3 - 6, 8, and 9 the data points refer to a typical computer run.

The base regime for 100-micron grains has a model layer of thickness D_L = 1 mm, identified as the MM regime. All craters of diameter 1 mm < D_C < 1 cm are considered, the smaller ones greatly predominating. Figure 3 shows the derived correlation between central track density and surface-exposure time after a typical layer residence time T_{MM} = 0.1 MT. Recall that model time MT most probably is equivalent to 1 My. The rectangle on the left represents the range of track densities for grains not yet exposed at the surface. The solid diagonal line represents the track density a grain would have if it accumulated tracks only while it was on the surface for a time t, while the dashed line represents the maximum density possible after time T_{MM}, thus enclosing the allowed zone. All grains with track density on the order of 10^8 cm^{-2} or more have resided directly on the surfa[illegible] All exposed grains have a central track density of at lea[illegible] cm^{-2} and will have strong track density gradients.

During a typical MM regime residence time of about 0.1 MT

nearly half of the grains will have been exposed at the surface. For these, cumulative exposure time distributions are shown in figure 4 for different residence times T_{MM}. Although only half of the grains in the 1 mm layer have been exposed the average exposure time is about 0.1 T_{MM}, indicated the effect of shielding by finer material. Note that shielding by larger grains on the order of 1 mm or more is excluded by the constraint that the simulated grains be within 1 mm of the surface, but will be accounted for in the next larger regime.

Figure 5 shows some track density parameters resulting from residence within the top 1 mm. Slopes greater than 1 in figure 5 reflect variation in a grain's depth due to impact gardening together with the steepness of the SF track production profile. Since grains which have a measurable track gradient as defined by Comstock (1977) must have resided within about 1 mm the parameters in figure 5 refer to that component P_{MM} of the central track density which would be related to an observed gradient.

The motion of 100-micron diameter grains is also followed in the next two larger regimes, for D_L = 1 cm denoted the CM regime and for D_L = 10 cm denoted the DM regime. For the CM regime we show in figure 6 some representative distributions of non-zero residence time within the 1 mm surface zone, identified with T_{MM}, for two typical 1 cm layer residence times T_{CM}. Only about a third of all grains have resided within 1 mm and these for an average time of about $T_{CM}/3$.

In figure 7 we plot parameters describing the tracks P_{CM} accumulated during residence between 1 mm and 1 cm depths. this represents the major contribution to central track density which

does not result in a track gradient in the grain. The minimum density refers mainly to grains that have remained near 1 cm. For those grains which have been cycled through the upper 1 mm surface zone the track densities indicated in figure 7 represent only part of the total accumulation and must be added to the tracks acquired within 1 mm (figure 5). Mostly these are grains which have resided in the upper part of the 1 cm layer and hence have higher partial densities P_{CM}; the median P_{CM} for this subset of well-irradiated grains is given by the dashed line in figure 7. Note that the maximum contribution to the total track density from residence below 1 mm (figure 7) tends to be comparable to the first quartile density contributed during residence within 1 mm (figure 5).

For the 10 cm (DM) regime figure 8 shows typical distributions for residence time $T_{CM} > 0$ within the top 1 cm for two residence times T_{DM} within 10 cm. The average values are about $T_{DM}/3$. The partial track density accumulated below 1 cm is obtained and taken into account, however it represents a factor of about ten less contribution to the total density than does residence between 1 mm and 1 cm.

Since most lunar soil sample intervals are centimeter or subcentimeter in size we are concerned more with the structure within the 10 cm regime, distinguishing samples in the mixed zone from those below the mixed zone. Some properties of the mixed zone are shown in figure 9 for the DM regime, similar properties hold in all regimes. In the bottom part of figure 9 is plotted the cumulative distribution of depths disturbed by impact events after a 10 cm layer residence time of 2 MT. In

all our plots the depth is measured relative to the current, observable surface not the initial surface, so it includes sites which have been recently excavated below the previously disturbed level and have only a thin mixed zone deposited since. This distribution was collected over a surface area of radius about 25 cm, a single core site would not reflect the broad spread even though it occurs quite localiy.

In the upper part of figure 9 we have plotted the correlation between depth and residence time within the surface zone for the same layer residence time and surface area as in the lower part. This plot makes clear that soil properties which depend on surface zone residence will be distributed equally throughout the mixed zone and that no general correlation with depth is to be expected.

This does not mean that the mixed zone will be found to be uniform at a particular core site, because the data in figure 9 were collected over an area much wider than the area of a sampled soil column. We find that over a typical core sample area there can be strong variations with depth. The variability of centimeter-interval samples in a soil column will reflect the variability of the CM regime as a function of T_{CM} allowed by the broad distribution shown in figure 8. Moveover there may be considerable variability on the millimeter scale reflecting the variability of the MM regime as a function of T_{MM}, also broadly distributed (figure 6). Evidence for strong variation of track densities over a few mm has been reported (e.g., Goswami et al., 1976).

MESS.2 results show that mm- and cm-scale variability can

easily be very local in origin. When such variation in the exposure and irradiation record is observed experimentally it should not in itself be considered sufficient evidence for a time variation in charged particle or micrometeoroid flux or for a different soil origin unless a definite correlation with depth can be established.

The time development of the median depth of the mixed zone is shown in figure 10 for each regime by the solid curves, which were collected over a area of radius 2.5 D_L. A regime was defined as a layer of depth D_L which was assumed to avoid local obliteration by large impact events for a time T_L. The median depth mixed by all events over a sufficiently wide area will be just the envelope of these curves indicated by the dashed line. The more one of the solid curves deviates from the dashed curve, the less likely it becomes that such a shallow depth will occur except very locally. Two things must be kept in mind when using plots such as these. First the mixed depth is broadly distributed, as indicated in the bottom part of figure 9, and may commonly be at least a factor of 2 in either direction from the median shown in figure 10. Secondly over a very small area such as is sampled by a soil core the mixed depth can vary erratically with time (either up or down) and will not necessarily follow in detail any of the curves shown, except statistically.

In an earlier model (Comstock, 1977, 1978) we assumed that all grains had resided within 1 mm of the surface and followed their motion as they were buried through the top few millimeters over a time of about 1 My which was called a surface exposure episode (SEE). The scenario assumed then is therefore equiva-

lent to grains residing in the mixed zone of our CM regime model which we see from figure 9 can be mixed to a few millimeters by local events in a time 1 MT. Although the current model treats detailed motion of the grains more accurately our earlier work is still approximately valid as a subset of our current results and probably represents a common situation. The current model covers a much broader range of soil residence conditions as well as deriving exposure and residence time distributions.

Sample synthesis--tracks.

The results obtained for each individual regime must now be combined to obtain the characteristics of a realistic soil sample containing grains which may have resided in more than one regime. We discuss first the distribution of particle track densities for 100-micron diameter grains which is representative of the grain size us· ·lly used for track studies.

The partial track densities accumulated during each regime as a function of residence time are first added together according to the derived distributions of residence times. This results in a series of time-dependent relations for the track parameters as a function of the shallowest regime in which the entire sample has resided. These relations for the minimum, first quartile, and median track densities are shown in figure 11. The time scales are lined up so average values correspond. It should be noted that since all the track distributions in this study are derived using a finite number of grains the minimum density in fact corresponds to about the first percentile. A similar caveat should be made for all experimental minimum

track densities. The true theoretical minimum density will always be somewhat less and not likely to be observed.

In figure 11 the curves marked MM describe a sample which has resided in the top millimeter but includes the contribution from residence below 1 mm. The MM curves should also apply well to any mm-sized sample taken from the mixed zone of a 1 cm surface layer. For mm-samples taken below this there may be an admixture of less-irradiated soil. Similarly the curves marked CM apply to cm-sized samples taken from a mixed zone up to several centimeters thick and the DM curves apply to dm-sized samples taken from a mixed zone several decimeters thick.

The data which lead to figure 11 can be presented another way in terms of a time vs. depth plot for a particular parameter as shown in figure 12 with the first quartile track density indicated by contour lines. The dashed line from figure 10 giving the overall mean mixed depth is also indicated by the dashed line in figure 12. The contour lines in the unmixed region reflect the shape of the track production profile in spite of some depth smearing due to gardening of the soil above. Within the mixed zone the contour lines become distorted and for mixed depths on the order of centimeters the very shallow depth dependence of the average quartile density is apparent.

The curves in figure 12 were derived assuming a statistically average sample, at a given sample site the contour lines within the mixed zone will depend on the actual series of impacts effecting the site sampled and on local mixed depth. We can see from figure 11 that any depth dependence that might have been expected within the mixed zone can be readily masked

by the wide variation in T_{MI} and T_{CM} allowed throughout the mixed zone, refer for example to the upper part of figure 9. Only within the uppermost 1 mm of soil is a depth dependence likely to become apparent because of the steep track production profile there. An interesting feature in figure 12 is the suggestion that the quartile track discontinuity at the bottom of the mixed zone becomes sharper as the zone becomes deeper.

In order to help calibrate our model time scale MT we have included in figure 12 a data point, indicated by the circled dot, obtained from the top of double drive tube 74002 collected at Shorty Crater. This is one of the clearest examples in the literature of an apparently fresh soil residing within the top 10 cm for the first time and, according to Crozaz (1979), is mixed to a depth of 6 cm over a time of 10 My. Crozaz finds a quartile track density within the mixed zone of about 3×10^6 cm^{-2}. Assuming that the Shorty Crater data represents an average sample it is consisent to assign 1 MT = 1 My, thus agreeing with the quartile track density shown in figure 12 as well as with our estimate above based on the crater production rate. This time scale also allows our mixed depths (dashed lines in figures 10 and 12) to match smoothly with mixed depths deduced from ^{22}Na and ^{26}Al profiles in lunar cores (Fruchter et al., 1976, 1978) and from I_s/FeO profiles (Morris, 1978).

Sample synthesis--exposure time.

We turn now to the derivation of average residence-time functions which would allow the calculation of other irradiation effects, solar wind implantation, FMR, etc. We are interested in the concentration C_i per unit mass of some given species i introduced at a rate F_i per unit area per unit time into soil grains residing either at the surface, denoted EX, or elsewhere within regime MM, CM, etc. We wish to obtain C_i as a function of residence time T_L within a soil layer of depth D_L. The desired concentration can be written in the following form:

$$(2)\quad C_i(T_L) = F_i \int_{m_a}^{m_b} I_X(T_L)_G \, (2f/pD_G) \, dm_G/M.$$

In this relation dm_G/M is the differential mass fraction for grains of diameter D_G. The factor $2f/pD_G$ gives the grain area exposed per unit mass for grains of diameter D_G where p is the grain density and f is the exposed area of a grain divided by its cross sectional area. The function $I_X(T_L)_G$ represents the effective average time spent within any zone X as a function of layer residence time T_L for grains of diameter D_G, where X and L may stand for EX, MM, CM, DM, etc. and the subscript G stands for D_G in centimeters. We use $I^*_X(T_L)_G$ to represent grains known to have come from the mixed zone of the layer L.

We are concerned here with the behavior of the model independently of the rates F_i and the exact distribution of grain sizes. Therefore we calculate effective area-time production functions G_X, for each grain size D_G, defined as follows:

(3a) $G_X(T_L)_G = (2f/p)[I_X(T_L)_G/D_G]$ for the whole layer L and

(3b) $G^*_X(T_L)_G = (2f/p)[I^*_X(T_L)_G/D_G]$ for the mixed zone of L.

We assume that f ideally is on the order of 1 and that 2f/p is

on the order of 1 in cgs units. Therefore in figures 13 to 18 I_X and I_X^* can be recovered from G_X and G_X^* by multiplying by the appropriate grain diameter in cm. In fact p will vary with grain composition and f will depend on grain shape, orientation, and partial shielding. Enhanced partial shielding by very small grains sticking to larger ones may be particularly important (Criswell and Basu, 1978; Housley, 1980) so it must be kept in mind that much uncertainty and some additional grain size dependence may still be buried in the factor f, as we discuss later.

Before we calculate the functions G_X we need to specify for each regime the relations for the distribution of non-zero surface-zone residence times and for the fraction of grains which have resided in the surface zone as a function of regime residence time. We will also need mechanisms for modifying the exposure time distributions to take into account the effective surface saturation of an accumulating species and the loss of grains by impact fragmentation at the surface.

From the MESS.2 Monte-Carlo simulations (e.g., figures 4, 6, 8) we find that in each regime the differential distribution of non-zero surface-zone residence times is described well by:

(4) $f_g(T_Z,T_L)_G = [\exp(-T_Z/K_TT_L)]/(K_TT_L)[1-\exp(-K_1/K_T)]$

for $0 < T_Z \leq K_1T_L$ and $f_g(T_Z,T_L)_G = 0$ for $T_Z > K_1T_L$.

where K_T is the main parameter, K_1 is a cutoff usually about 1. In a base regime T_Z stands for the actual space-exposure time t. The fraction of grains which have been cycled through the surface zone is approximately given for typical T_L by the form:

(5) $f_e(T_L)_G = f_m\,[1-\exp(-T_L/T_r)]$ for $T_r/3 \lesssim T_L \lesssim 3T_r$.

For $T_L >> T_r$ the fraction f_e will continue to increase slowly

but this has little effect on the results. Parameters f_m and T_r define a mixing efficiency and time constant, respectively. The values found for the various constants are given in table 1 for each regime. Note that grains residing in their base regime behave somewhat differently than do smaller grains in that regime, due to the graininess of the model soil.

The statistical method outlined in the following paragraphs represents an approximation to the actual grain depth history within a surface zone. MESS.2 was originally designed to follow more precisely the grain depths in each surface zone by using smaller scale statistics continuously during the computer run for a given regime. This was found to be very time consuming without giving significantly different results than the methods described in this paper. The effect was to alter slightly the detailed shapes of the exposure and track distributions but not the average exposure time or the maximum and minimum irradiation levels; the additional complexity is not justified in view of current uncertainties in other model parameters.

We now derive the average residence time functions I_X in the following manner. For a given grain size we first start with the base regime, for 100-micron diameter grains this is the MM regime. Since the desired characteristics of grains anywhere within the mixed zone reflect residence in the surface zone we first average over possible surface-zone residences. The average space-exposure time for grains from the mixed zone of the MM regime in the absence of fragmentation and saturation is:

$$(6)\quad I^{*}_{EX}(T_{MM})_{.01} = \int_0^{T_{MM}} t\, f_g(t, T_{MM})_{.01}\, dt.$$

If we sample the entire 1 mm layer then we must add the unmixed

grains as well by renormalizing the integral as follows:

(7) $I_{EX}(T_{MM})_{.01} = f_e(T_{MM})_{.01}\ I^*_{EX}(T_{MM})_{.01}$.

In equations 6 and 7 the functions f_g and f_e use parameter values from table 1 for 100-micron grains in the MM regime.

Now we must correct this to take into account fragmentation and saturation effects. We assume that the fraction of grains surviving loss by fragmentation for a surface time t is:

(8) $f_1(t)_G = \exp(-t/T_1(D_G))$.

We approximate grain-surface saturation processes by multiplying the integrand in equation 6 by a saturation function given by:

(9) $f_r(t) = (T_s/t)[1-\exp(-t/T_s)]$.

The functions I_X and I^*_X will then represent effective average times with saturation built in unless T_s goes to infinity.

With the correction factors for grain fragmentation and possible saturation included the average exposure time in equation 6 for the mixed zone of the top 1 mm becomes:

$$(10)\quad I^*_{EX}(T_{MM})_{.01} = (1/F)\int_0^{T_{MM}} t\ f_r(t)\ f_1(t)_{.01}\ f_g(t,T_{MM})_{.01}\ dt$$

where $F = \int_0^{T_{MM}} f_1(t)_{.01}\ f_g(t,T_{MM})_{.01}\ dt$.

Equation 7 for the whole 1 mm layer becomes:

(11) $I_{EX}(T_{MM})_{.01} = [Ff_e/(1-f_e+Ff_e)]\ I_{EX}{}^*(T_{MM})_{.01}$

where f_e is $f_e(T_{MM})_{.01}$ and the fragmented grains have been removed from the 100-micron grain size population.

We now construct the effective average exposure time for 100-micron grains that reside in the upper 1 cm of soil, simulated by the CM regime. For grains from the mixed zone of a 1 cm layer we ideally would average over 1 mm surface-zone residence episodes as follows (suppressing subscripts EX and .01

for clarity:)

$$(12a)\quad I^*(T_{CM}) = p_1(T_{CM}) \int_0^{T_{CM}} I(T_{MM})\, f'_g(T_{MM},T_{CM})\, dT_{MM} +$$

$$p_2(T_{CM}) \int_0^{T_{CM}} \int_0^{T_{MM}} [I(T'_{MM})+I(T_{MM}-T'_{MM})]\, f'_g(T'_{MM},T_{CM})$$

$$f'_g(T_{MM}-T'_{MM},T_{CM})\, dT'_{MM}\, dT_{MM} + \ldots\ldots$$

where the first term is contributed by that fraction of grains p_1 which have resided only once within the 1 mm surface zone, the second term is contributed by that fraction of grains p_2 which have resided twice and only twice within the surface zone, and so on for higher order terms. The distribution f'_g gives the frequency of surface-zone residence times for individual episodes within the surface zone, as a function of layer time.

In two independent cases equation 12a will reduce to the much simpler form given by:

$$(12b)\quad I^*_{EX}(T_{CM}).01 = \int_0^{T_{CM}} I_{EX}(T_{MM}).01\, f_g(T_{MM},T_{CM}).01\, dT_{MM}.$$

where f_g is the total surface-zone residence time distribution such as that shown in figure 6. The two cases occur under the following conditions, either:

(a) $p_n = 0$ for all $n > 1$, so that $p_1 = 1$ and $f'_g = f_g$; or else

(b) $I_{EX}(T_{MM})$ is proportional to T_{MM}, so $I(T')+I(T-T')=I(T)$

which along with the definition of f_g in terms of f'_g gives equation 12b from 12a.

Our MESS.2 Monte-Carlo calculations give the distributions f'_g and fractions p_n so equations 12a and 12b can be compared. We find that for low values of T_{CM} the condition for case (a) are generally satisfied (but not case b). For higher T_{CM} case

(b) is nearly satisfied in the absence of grain fragmentation or saturation, although two or three surface-zone episodes become common; on the other hand if $I_{EX}(T_{MM})$ becomes saturated then multiple surface-zone episodes become ineffective again due to losses or grain-surface saturation, and the condition for case (a) is effectively approached instead. In all cases equation 12b becomes a useful approximation.

When the entire 1 cm layer is sampled we will have:

(13) $I_{EX}(T_{CM})_{.01} = f_e(T_{CM})_{.01}\ I^*_{EX}(T_{CM})_{.01}$.

If we need the average time spent within 1 mm as a function of T_{CM}, for samples from the mixed zone of the 1 cm layer, we use:

(14) $$I^*_{MM}(T_{CM})_{.01} = \int_0^{T_{CM}} T_{MM}\ f_g(T_{MM},T_{CM})_{.01}\ dT_{MM}.$$

For the whole layer we use:

(15) $I_{MM}(T_{CM})_{.01} = f_e(T_{CM})_{.01}\ I^*_{MM}(T_{CM})_{.01}$.

In equations 12b through 15 the functions f_g and f_e use the parameters in table 1 for 100-micron grains in the CM regime.

Similar relations can be obtained for samples from a 10 cm layer. The most useful of these give average space-exposure time and average 1mm-layer residence time for samples from the mixed zone of the 10 cm layer approximated respectively by:

(16) $$I^*_{EX}(T_{DM})_{.01} = \int_0^{T_{DM}} I_{EX}(T_{CM})_{.01}\ f_g(T_{CM},T_{DM})_{.01}\ dT_{CM}$$ and

(17) $$I^*_{MM}(T_{DM})_{.01} = \int_0^{T_{DM}} I_{MM}(T_{CM})_{.01}\ f_g(T_{CM},T_{DM})_{.01}\ dT_{CM}$$

where the parameters from table 1 for 100-micron grains in the DM regime are used in f_g. Equations 16 and 17 are used for the same reasons discussed in reference to equations 12a and 12b.

If the functions I_X found above are now divided by grain diameter D_G = 0.01 cm we obtain the effective area-time production functions G_X as discussed earlier. Production functions were derived similarly for representative grain diameters D_G = 0.001 and 0.1 cm. Some of these results are shown in figures 13 to 18. In all of these figures the curves labelled A, B, or C refer to different assumptions for the fragmentation time constant T_1 and the saturation time constant T_s as defined earlier. The curves labelled A were derived assuming no fragmentation or saturation. The curves labelled B assume only grain fragmentation, using values for T_1 of 0.3, 0.2, 0.1 MT for 10-micron, 100-micron, and 1 mm diameter grains respectively (except in figure 18 discussed later). With an identification of 1 MT = 1 My these correspond to the shorter fragmentation times discussed earlier. The curves labelled C assume both these same fragmentation losses plus a surface saturation time of T_s = 0.01 MT (except in figure 18) again corresponding to a plausible value discussed above for 1 MT = 1 My.

Figures 13 to 15 give the effective production functions for direct space exposure. In figure 13 we plot $G^*_{EX}(T_{CM})_G$ describing mm-sized samples taken from the mixed zone of a 1 cm surface layer, figure 14 shows $G_{EX}(T_{CM})_G$ describing the entire 1 cm layer including unexposed grains below the mixed zone, and figure 15 shows $G^*_{EX}(T_{DM})_G$ describing a 1 cm sample from the mixed zone of a 10 cm layer, all as functions of the whole layer residence time. Figure 16 gives $G_{IM}(T_{DM})_G$, the production function for residence within 1 mm for grains in a 1 cm sample taken from the mixed zone of a 10 cm layer.

DISCUSSION

Figures 13 - 16 all have important features in common. In the absence of fragmentation or saturation (curves A) 100-micron diameter grains show a lower production function than either 10-micron or 1 mm diameter grains. This results from a combination of effects: A larger fraction of grains (our model matrix) is available to lightly cover 100-micron grains compared to 10-micron grains in their respective base regimes, i.e. very close to the surface. 1 mm grains would be even more readily covered by finer material but the steeper size-frequency distribution of craters (corresponding to >500-micron diameter rock pits) in the CM base regime for 1 mm grains gives them a better chance to be exposed by shallow events while residing very near the surface.

In the presence of grain fragmentation (curves B) the effect of fragmentation by direct impact while on the surface is much stronger for 1 mm grains due to longer surface exposure but similar fragmentation time constants. In fact the loss of 1 mm grains is so great that the production factor for the whole 1 cm layer shown in figure 14 becomes more effected by the unexposed grains below the mixed zone and begins to decrease with time, as the mixed zone is depleted in 1 mm grains.

When our presumed saturation time is also included (curves C) the production functions become well separated by grain size in a more surface-correlated manner. Note that the production function for 1 mm grains can reach an effective saturation due to fragmentation alone and all grain size fractions can reach saturation within typical residence times in the presence of our assumed saturation time $T_s = 0.01$ MT.

For processes requiring only residence within the top 1 mm, governed by production functions G_{MM} and G^*_{MM} (e.g. figure 16), fragmentation losses and grain saturation have much less effect except for soil particles whose diameter approaches or exceeds the depth of the production zone, which is 1 mm in this case.

We emphasize that saturation of a production function G_X represents an average over all grains in the sample and does not mean that all grains are saturated individually. In the less-mature soils modeled here at least half of the grains remain unexposed at the surface, others will reach saturation on the exposed portion of their surfaces.

In figure 17 we have summarized the apparent grain size dependence D_G^{-n} implied by production functions $G^*_X(T_{DM})_G$. The solid lines give $n = \log_{10}[G^*_X(T_{DM})_{.001}/G^*_X(T_{DM})_{.01}]$ and the dashed lines give $n = \log_{10}[G^*_X(T_{DM})_{.01}/G^*_X(T_{DM})_{.1}]$ where X refers to EX and MM. Since all grains tend to reside equally within the first 1 mm the functions G^*_{MM} show strong surface correlation (n = 1). The production functions G^*_{EX} for space exposure tend to be more volume correlated (n = 0) for short times. As time goes on both fragmentation and saturation cause G^*_{EX} to become more surface correlated, and this effect begins earlier for larger grains as suggested by Criswell (1975). These results apply to the early in-situ development of less-mature soil. Mature soil will have been subjected to additional equilibrating effects of agglutination, comminution and mixing.

To obtain the results described through figure 17 we have assumed a certain set of fragmentation and saturation time constants. However if the time scale changes due to a variation

in micrometeoroid flux or if the solar wind flux varies, then the effects of fragmentation and saturation as functions of time may be different. For example if for a given sample the appropriate time scale should be represented by 1 MT = 10 My due to a factor of 10 decrease in the micrometeoroid flux, then T_1 would maintain the same value in units of MT (less fragmentation also) but T_s would remain 0.01 My corresponding to 0.001 MT. For 100-micron grains this would produce the curve D in figure 15, saturating at a factor of 10 below the corresponding curve C for 1 MT = 1 My. Curves A and B would remain the same in this case.

However if the time scale were to change to 1 MT = 10 My due to a reduction in crater size in a soil of greater cohesion, then both the fragmentation and saturation time constants will decrease by a factor of 10 in units of MT. This will produce the situation shown in figure 18 for the effective production function $C^*_{EX}(T_{DM})_G$ in the mixed zone of a 10 cm layer, where T_1 = 0.03, 0.02, and 0.01 MT for 10-micron, 100-micron, and 1 mm grains, respectively, and T_s = 0.001 MT. In this case all grain size fractions can reach an effective saturation during typical residence times due to fragmentation alone. Note that for 1 MT = 10 My the typical residence times become 10 times longer than for 1 MT = 1 My. These properties may be useful in detecting time variations or variations in soil mechanical properties. In this context note also that all track density parameters are proportional to the model time unit MT.

In correlating track results with production functions C_X we must keep in mind that the minimum, quartile, and median track densities are strongly controlled by the less irradiated

grains in a sample while the production factors are usually controlled by the more irradiated grains. Therefore in a sample which mixes grains with the allowed wide range of local surface history there may be considerable variability in a correlation between tracks and noble gas concentration, for example. For a statistically average sample however the track parameters marked MM in figure 11 using the T_{CM} time axis should correspond to production factors given in figures 13 and 14 for 100-micron grains, while the curves marked CM in figure 11 using the T_{DM} time axis should correspond to the production functions in figures 15, 16, and 18 for 100-micron diameter grains.

It is beyond the scope of this paper to compare our results in detail with the many measured soil samples. Judging from the Shorty Crater data (Crozaz, 1979) and other track measurements the track parameters derived here seem reasonable for the postulated time scale 1 MT = 1 My. The situation for solar wind concentration is more complicated, being dependent on various mineral- and species-specific effects (Pillinger, 1979). Our production factors seem reasonable in terms of average gas concentrations, however as Wieler et al. (1980) have pointed out there is some difficulty when the distribution for individual grains is considered. Kirsten et al. (1971) have also measured gas concentrations in individual grains.

Less-mature soils derived here have fewer exposed grains than expected for mature soils. However, a gas-poor soil 60051 was found by Wieler et al. (1980) to contain some noble gas concentration in all 83 measured grains, apparently implying universal exposure for less-mature soils as well, contrary to

our model. These authors also measured track densities in 64 grains from the same sample and found a median central density of less than 10^7 cm^{-2} and only 19% with densities greater than 10^8 cm^{-2}. These values are consistent with our model track results but inconsistent with universal space exposure. Wieler et al. (1980) suggert that grain fragmentation is responsible for the lack of track density gradients which they also observe, but fragments which lack such gradients have never been exposed and should lack SW gas concentration as well.

It may therefore be necessary to find a mechanism yielding a surface concentration of SW elements in most grains without all being exposed to space. Such a mechanism could involve the intermediate action of small grains. Criswell and Basu (1978) show that the size fraction less than 4 microns is generally capable of covering all larger grains which, together with the intergrain forces acting on soil grains (Housley, 1980) will make it hard to avoid partial covering of most larger grains on the surface. In their study of microcraters on soil grains Poupeau et al. (1975, 1978) find that even grains from mature soils have pits only on a small portion of their surfaces.

If smaller grains coat part the surfaces of otherwise exposed larger grains then they will acquire much of the SW gas. During subsequent burial through the uppermost few millimeters they will be subject repeatedly to shock compression by micrometeoroid impacts (Stöffler et al., 1975) which dissipate a considerable fraction of their energy collapsing pore spaces between the soil grains (Braslau, 1970). Even weak shock can result in soil compaction and grain deformation, with minor

melting (Schaal and Hörz, 1980). It seems plausible that during this process gas-loaded fine material coating some of the larger grains could impart a concentration of SW atoms to the remaining unexposed grains residing near the surface. The process may become masked by subsequent exposure effects as the soil matures. The problem requires more work on the nature of grain-interface processes during soil compaction and involves a better understanding of the depth profiles of SW elements in individual grains (e.g., Müller et al., 1976; Zinner et al., 1978; Warhaut et al., 1979).

If grains can acquire a SW concentration while residing within only the top millimeter of soil then it is clear from figure 17 that surface correlation can be obtained even for an immature soil which is incompletely exposed. In addition if larger grains are subject to enhanced shielding due to intergrain forces while residing on the surface then their exposure area controlled by the parameter f in equations 2 and 3 will be much less. Derived production functions G_X and G_X^* will then be proportional to $f < 1$ and individual grains can reach microscopic saturation (Wieler et al., 1980) at a total concentration much less than that for fully-exposed grains. Since the intergrain forces primarily control smaller grains ($\lesssim$ 10 microns, apparently) the smaller value of f should still be fairly constant for larger grains and increase again only for the smaller grains, as argued qualitatively by Housley (1980).

In summary, we have developed a model which allows us to derive distributions of track density, surface exposure times, and residence times within various zones as functions of grain

size, sample size and depth, and residence time. The results apply to samples which have resided within the top 10 cm for one time only and thus refer to relatively less-mature soils. Older surface layers which have been quickly buried deep enough to preserve their surface history undisturbed will also be described by these results. Data from Shorty Crater has been used to help calibrate the model time scale, yielding reasonable track distributions and average exposure times. Important questions remain concerning the distribution of solar wind elements among the grains in less-mature samples and concerning the role of very fine soil material in controlling grain-size dependences and solar wind gas distribution. This work can be extended to apply to mature soils which may have resided several times within the top 10 cm.

Acknowledgements--We thank I. Langevin for useful discussions concerning features of the Monte-Carlo model. This work was supported by NASA under Contract NASW-3273.

References.

Arnold, J., Monte Carlo simulation of turnover processes in the lunar regolith, Proc. Lunar Sci. Conf. 6th, pp. 2375-2395, Pergamon, 1975.

Becker, R. H., Does application of the Rosiwal Principle to lunar soils require that concentrations of solar wind-implanted species be grain-size independent? Earth Planet. Sci. Lett. 34, 136-140, 1977.

Bogard, D. D., Effects of soil maturation on grain size-dependence of trapped solar gases, Proc. Lunar Sci. Conf. 8th, pp. 3705-3718, Pergamon, 1977.

Borg, J., Comstock, G. M., Langevin, Y., and Maurette, M., A Monte Carlo model for the exposure history of lunar dust grains in the ancient solar wind, Earth Planet. Sci. Lett. 29, 161-174, 1976.

Braslau, D., Partitioning of energy in hypervelocity impact against loose sand targets, J. Geophys. Res. 75, 3987-3999, 1970.

Comstock, G. M., On deciphering the particle track record of lunar regolith history, J. Geophys. Res. 82, 357-367, 1977.

Comstock, G. M., Miniregoliths I: Dusty lunar rocks and lunar soil layers, Proc. Lunar Planet. Sci. Conf. 9th, pp. 2557-2577, Pergamon, 1978.

Comstock, G. M., Miniregoliths and Monte-Carlo modeling, in Lunar and Planetary Science X, pp. 229-231, The Lunar and Planetary Institute, Houston, 1979.

Comstock, G. M., Miniregoliths II: Anatomy of lunar surface soil, in Lunar and Planetary Science XII, pp. 169-171, The

Lunar and Planetary Institute, Houston, 1981.

Criswell, D. R., The Rosiwal Principle and the regolithic distributions of solar-wind elements, Proc. Lunar Sci. Conf. 6th, pp. 1967-1987, Pergamon, 1975.

Criswell, D. R., and Basu, A., Rosiwal Principle and surface exposure of lunar soil grains, in Lunar and Planetary Science IX, pp. 197-199, The Lunar and Planetary Institute, Houston, 1978.

Crozaz, G., Regolith reworking at Shorty Crater, Proc. Lunar Planet. Sci. Conf. 10th, pp. 1381-1384, Pergamon, 1979.

Duraud, J. P., Langevin, Y., Maurette, M., Comstock, G. M., and Burlingame, A. L., The simulated depth history of dust grains in the lunar regolith, Proc. Lunar Sci. Conf. 6th, pp. 2397-2415, Pergamon, 1975.

Eugster, O., Eberhardt, P., Geiss, J., Grögler, N., Jungck, M., and Mörgeli, M., Solar-wind-trapped and cosmic-ray-produced noble gases in Luna 20 soil, Proc. Lunar Sci. Conf. 6th, pp. 1989-2007, Pergamon, 1975.

Flavill, R. P., Carey, W. C., McDonnell, J. A. M., Ashworth, D. G., and Allison, R. J., Progress in defining the solar wind sputter rate on protoplanets and interplanetary matter, Planet. Space Sci., 28, 511-524, 1980.

Fruchter, J. S., Rancitelli, L. A., and Perkins, R. W., Recent and long-term mixing of the lunar regolith based on ^{22}Na and ^{26}Al measurements in Apollo 15, 16, and 17 deep drill stems and drive tubes, Proc. Lunar Sci. Conf. 7th, pp. 27-39, Pergamon, 1976.

Fruchter, J. S., Rancitelli, L. A., Evans, J. C., and Perkins, R. W., Lunar surface processes and cosmic ray histories over

the past several million years, Proc. Lunar Planet. Sci. Conf. 9th, pp. 2019-2032, Pergamon, 1978.

Gault, D. E., Hörz, F., Brownlee, D. E., and Hartung, J. B., Mixing of the lunar regolith, Proc. Lunar Sci. Conf. 5th, pp. 2365-2386, Pergamon, 1974.

Gault, D. E., and Wedekind, J. A., Experimental hypervelocity impact into quartz sand--II, Effects of gravitational acceleration, in Impact and Explosion Cratering, edited by D. J. Roddy, R. O. Pepin, and R. B. Merrill, pp. 1231-1244, Pergamon, 1977.

Goswami, J. N., Braddy, D., and Price, P. B., Microstratigraphy of the lunar regolith and compaction ages of lunar breccias, Proc. Lunar Sci. Conf. 7th, pp. 55-74, Pergamon, 1976.

Hörz, F., Schneider, E., and Hill, R. E., Micrometeoroid abrasion of lunar rocks: A Monte-Carlo simulation, Proc. Lunar Sci. Conf. 5th, pp. 2397-2412, Pergamon, 1974.

Hörz, F., Brownlee, D. E., Fechtig, H., Hartung, J. B., Morrison Morrison, D. A., Neukum, G., Schneider, E., Vedder, J. F., and Gault, D. E., Lunar microcraters: Implications for the micrometeoroid complex, Planet. Space Sci. 23, 151-172, 1975.

Housley, R. M., Toward a model of grain surface exposure in planetary regoliths, in Proc. Conf. Ancient Sun, edited by R. O. Pepin, J. A. Eddy, and R. B. Merrill, pp. 401-410, The Lunar and Planetary Institute, 1980.

Kirsten, T., Steinbrunn, F., and Zahringer, J., Location and variation of trapped rare gases in Apollo 12 lunar samples, Proc. Lunar Sci. Conf. 2nd, pp. 1651-1669, MIT Press, Cambridge, 1971.

Morris, R. V., In situ reworking (gardening) of the lunar

surface: Evidence from the Apollo cores, Proc. Lunar Planet. Sci. Conf. 9th, pp. 1801-1811, Pergamon, 1978.

Morris, R. V., Origins and size distribution of metallic iron particles in the lunar regolith, Proc. Lunar Planet. Sci. Conf. 11th, pp. 1697-1712, Pergamon, 1980.

Morris, R. V., Gose, W. A., and Laurer, H. V., Jr., Depositional and surface exposure history of the Shorty Crater core 74001/2: FMR and magnetic studies, Proc. Lunar Planet. Sci. Conf. 9th, pp. 2033-2048, Pergamon, 1978.

Morrison, D. A., and Zinner, E., 12054 and 76215: New measurements of interplanetary dust and solar flare fluxes, Proc. Lunar Sci. Conf. 8th, pp. 841-863, Pergamon, 1977.

Müller, H. W., Jordan, J., Kalbitzer, S., Kiko, J., and Kirsten, T., Rare gas ion probe analysis of helium profiles in individual lunar soil particles, Proc. Lunar Sci. Conf. 7th, pp. 937-951, Pergamon, 1976.

Pillinger, C. T., Solar-wind exposure effects in the lunar soil, Rep. Prog. Phys., 42, 897-961, 1979.

Poupeau, G., Christophe-Michel-Levy, M., Mandeville, J. C., Johnson, J., and Romary, Ph., Microcrater and solar-flare track maturation of the lunar regolith, in Mare Crisium: The View from Luna 24, edited by R. B. Merrill and J. J. Papike, pp. 137-155, Pergamon, 1978.

Poupeau, G., Walker, R. M., Zinner, E., and Morrison, D. A., Surface exposure history of individual crystals in the lunar regolith, Proc. Lunar Sci. Conf. 6th, pp. 3433-3448, Pergamon, 1975.

Schall, R. B., and Hörz, F., Experimental shock metamorphism of lunar soil, Proc. Lunar Planet. Sci. Conf. 11th, pp. 1679-

1695, Pergamon, 1980.

Signer, P., Baur, H., Derksen, U., Etique, Ph., Funk, H., Horn, P., and Wieler, R., Helium, neon, and argon records of lunar soil evolution, Proc. Lunar Sci. Conf. 8th, pp. 3657-3684, Pergamon, 1977.

Stöffler, D., Gault, D. E., Wedekind, J., and Polkowski, G., Experimental hypervelocity impact into quartz sand: Distribution and shock metamorphism of ejecta, J. Geophys. Res. 80, 4062-4077, 1975.

Tamhane, A. S., and Agrawal, J. K., Diffusion of rare gases of solar wind origin from lunar fines as bubbles, Earth Planet. Sci. Lett. 42, 243-250, 1979.

Vedder, J. F., Craters formed in mineral dust by hypervelocity microparticles, J. Geophys. Res. 77, 4304-4309, 1972.

Walker, R., and Yuhas, D., Cosmic ray track production rates in lunar materials, Proc. Lunar Sci. Conf. 4th, pp. 2379-2389, Pergamon, 1973.

Warhaut, M., Kiko, J., and Kirsten, T., Microdistribution patterns of implanted rare gases in a large number of individual lunar soil particles, Proc. Lunar Planet. Sci. Conf. 10th, pp. 1531-1546, Pergamon, 1979.

Wieler, R., Etique, Ph., Signer, P., and Poupeau, G., Record of the solar corpuscular radiation in minerals from lunar soils: A comparative study of noble gases and tracks, Proc. Lunar Planet. Sci. Conf. 11th, pp. 1369-1393, Pergamon, 1980.

Zinner, E., Dust, S., Chaumont, J., and Dran, J. C., Surface concentrations of Mg, Ti, Fe and surface features in individual plagioclase crystals from lunar soil samples. Proc. Lunar Planet. Sci. Conf. 9th, pp. 1667-1686, Pergamon, 1978.

TABLE 1

MESS.2 Model Layers and Derived Parameters

	---- Base Regimes----			-- Larger Regimes --		
	DMM	MM	CM	MM	CM	DM
D_L (cm)	0.01	0.1	1	0.1	1	10
D_Z (cm)	0.001	0.01	0.1	0.01	0.1	1
D_G (cm)	0.001	0.01	0.1	<0.01	<0.1	<1
K_T	0.50	0.16	0.40	0.25	0.40	0.75
K_l	1.0	0.4	0.8	1.0	0.9	1.0
f_m	0.50	0.50	0.60	0.35	0.30	0.22
T_r (MT)	0.02	0.026	0.35	0.01	0.12	0.90

Figure Captions

1. A schematic representation of depth zones defined by MESS.2 for a model regime. The model layer for a given regime corresponds to the surface zone for the next larger size regime.
2. The ejecta origin map developed for MESS.2. H_c and R_c are the central depth and rim radius, respectively, of the excavated volume of the crater, h and r are the initial depth and radial distance, respectively, of a given soil particle, and r_a is the final radial distance of the ejected particle.
3. A correlation between central track density and surface exposure time derived by MESS.2 for grains of diameter 100 microns after a typical residence time T_{MM} within the top 1 mm of soil. The diagonal and dashed lines indicate allowed lower and upper limits, respectively, to the track density and the thin rectangle represents grains not directly exposed. In all figures 1 MT is a model time unit most likely equal to 10^6 years (1 My), unless otherwise noted.
4. Typical cumulative distributions of space-exposure time t derived by MESS.2 for grains of diameter 100 microns after a residence time T_{MM} within the top 1 mm of soil, for those grains which have been exposed to space ($t > 0$).
5. Track parameters derived by MESS.2 characterizing tracks accumulated in the center of 100-micron diameter grains during residence within the top 1 mm of soil, as functions of that residence time. MIN, Q, MED, 3Q, and MAX refer to minimum, first quartile, median, third quartile, and maximum track densities, respectively.

6. Typical cumulative distributions of non-zero residence times T_{MM} within the top 1 mm of soil derived by MESS.2 for grains of diameter 100 microns after a residence time T_{CM} within the top 1 cm.

7. Track parameters derived by MESS.2 characterizing tracks accumulated in the center of 100-micron diameter grains while residing at depths between 1 mm and 1 cm below the soil surface, as functions of grain residence time within the top 1 cm. The dashed line gives the median track density accumulated at depths between 1 mm and 1 cm for those grains which have also resided within the top 1 mm, and hence represents a partial density to be added to the track densities shown in figure 5.

8. Typical cumulative distributions of non-zero residence times T_{CM} within the top 1 cm of soil derived by MESS.2 for grains of diameter 100 microns after a residence time T_{DM} within the top 10 cm.

9. Some properties of the mixed zone of a 10 cm surface layer derived by MESS.2 after a typical layer residence time T_{DM}. The lower portion shows the cumulative distribution for depths of the mixed zone, collected over an area of radius 25 cm. The upper portion is a scatter diagram for 100-micron diameter grains showing their depth plotted against their surface-zone residence time T_{CM} (total time spent within the top 1 cm). No general correlation of T_{CM} with depth is evident.

10. The time development of the median depth of the mixed zone derived by MESS.2 for certain regimes. The solid curves labelled MM, CM, and DM refer to 1 mm, 1 cm, and 10 cm thick

surface layers, respectively, which have locally survived destruction by relatively large impacts for residence times $T_L = T_{MI}$, T_{CI}, and T_{DM}, respectively. The dashed curve includes all sites, without the survival constraint.

11. The minimum, first quartile, and median central track densities derived by MESS.2 for a sample of 100-micron diameter grains as functions of residence time within the shallowest depth regime in which the entire sample has resided. Track contributions from greater depths are included according to derived residence time distributions. The time scales are lined up so that average values will correspond.

12. Contours of equal quartile track density derived by MESS.2 for 100-micron diameter grains in a statistically average layer as functions of depth and layer residence time. The dashed curve gives the median depth of the mixed zone as in figure 10. A data point for the top of double drive tube 74002 from Shorty Crater (circled dot) helps to calibrate the model time unit 1 MT as 10^6 years (1 My).

13. Effective area-time-per-mass production factors for surface exposure derived by MESS.2 for typical grain diameters D_G as functions of residence time within the top 1 cm. These curves are applicable to samples taken from the few-millimeters thick mixed zone of the 1 cm layer. In figures 13 - 18 all curves labelled A do not include grain fragmentation or surface saturation, curves labelled B include a loss by fragmentation due to direct impacts, curves labelled C include fragmentation plus an effective exposure time corrected for a grain-surface saturation effect.

14. Effective area-time-per-mass production factors for surface exposure as in figure 13 except that these curves apply to a sample taken from the entire 1 cm surface layer.

15. Effective area-time-per-mass production factors for surface exposure derived by MESS.2 as functions of residence time within the top 10 cm. These curves apply to samples taken from the few-centimeters thick mixed zone of the 10 cm layer. The curve labelled D replaces curve C for D_G = 100 microns in the case of a factor of 10 decrease in the micrometeoroid flux; curves A and B are unchanged in this case but the probable value of the model time unit 1 MT would become 10 My.,

16. Effective area-time-per-mass production factors for residence within the top 1 mm derived by MESS.2 as functions of residence time within the top 10 cm. These curves apply to samples taken from the mixed zone of the 10 cm layer. Effective residence times within 1 mm are much less controlled by surface fragmentation and grain saturation except for soil particles whose diameter approaches or exceeds the depth of the assumed production zone.

17. Assuming that the area-time-per-mass production factors follow a grain size dependence D_G^{-n} where n may be slowly varying, we approximate n in two size intervals, 10 microns to 100 microns (solid curves), and 100 microns to 1 mm (dashed curves) from the data shown in figures 15 and 16, as functions of residence time within the top 10 cm. As before, A refers to no fragmentation or saturation, B includes fragmentation loss at the surface, and C includes fragmentation plus an effective exposure time due to grain saturation.

18. Effective area-time-per-mass production factors for surface exposure as in figure 15 except that here the probable value of the model time unit 1 MT becomes 10 My due to a reduction in crater size by a factor of about 2, in a soil with greater cohesion, for example. Both fragmentation and saturation will strongly effect all grain sizes in this situation.

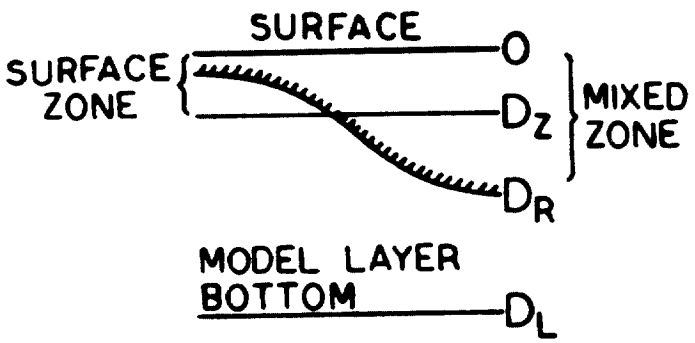

Fig 1

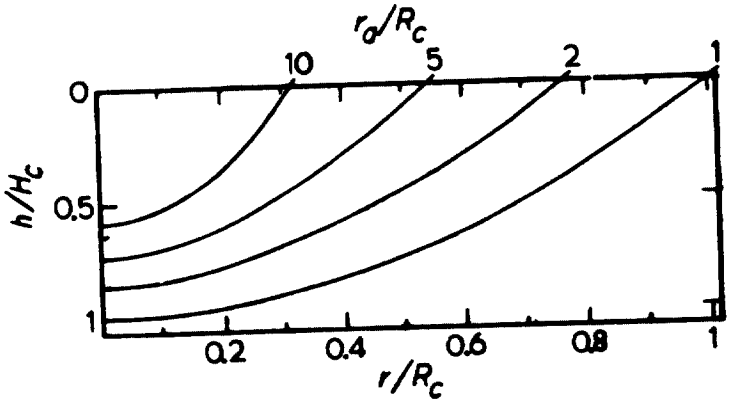

Fig 2

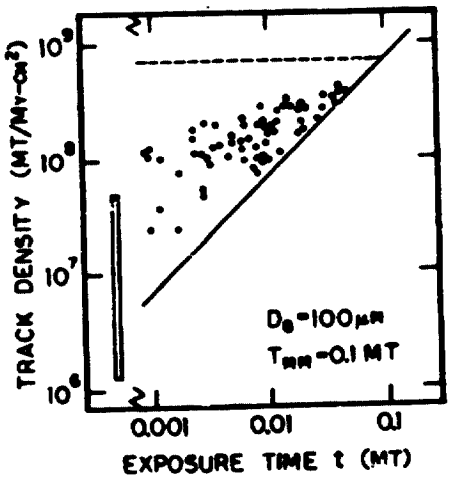

Fig 3

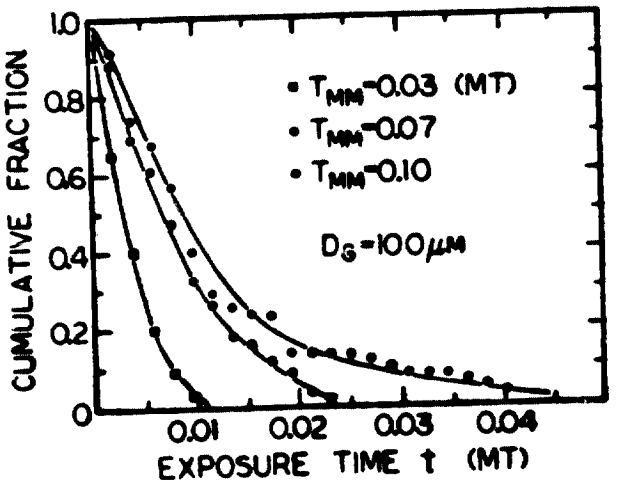

Fig 4

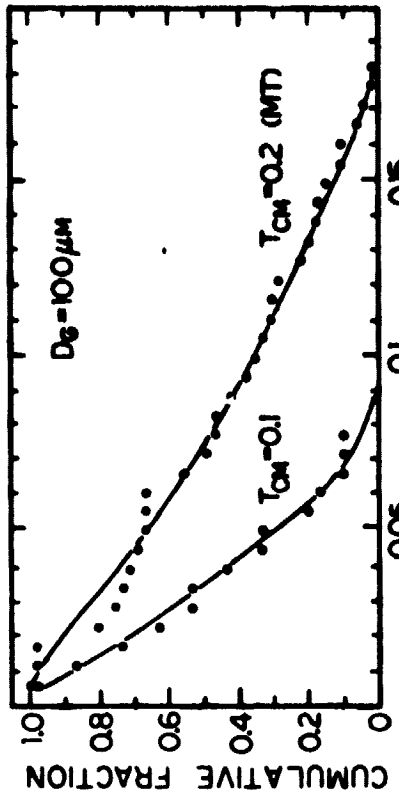

Fig 6

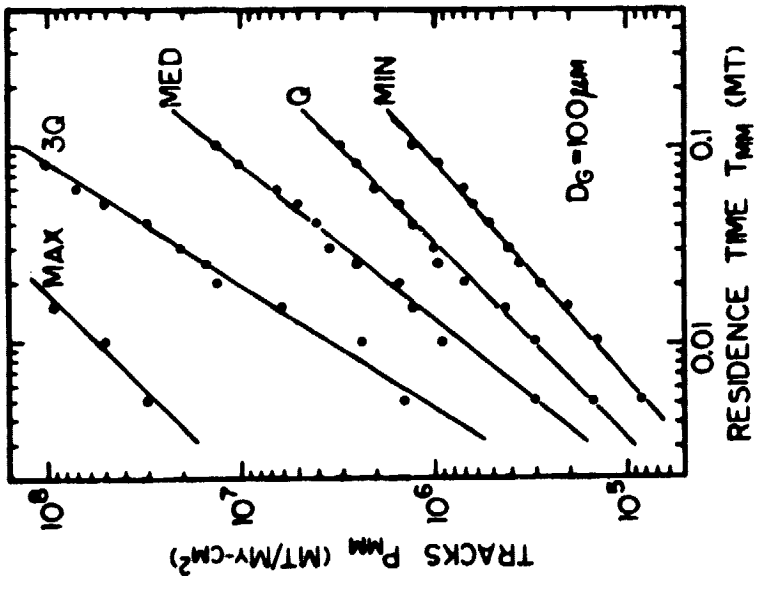

Fig 5

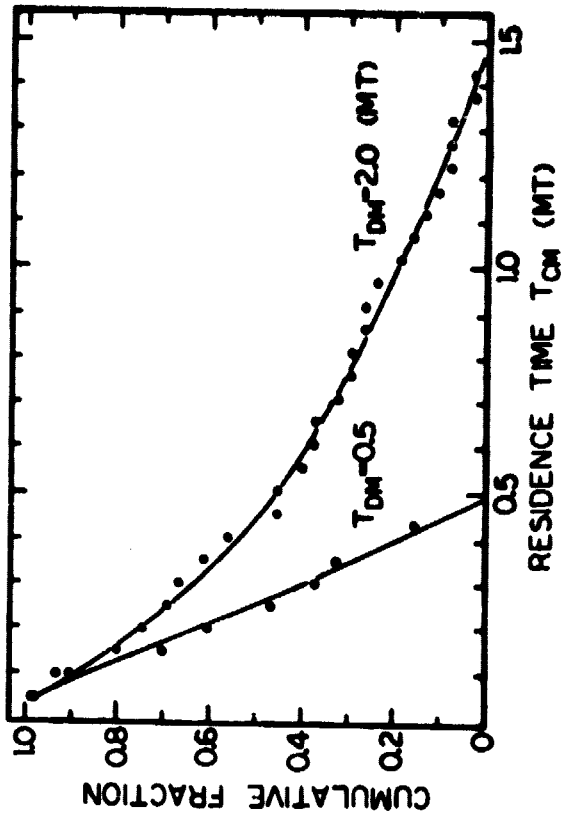

Fig 8

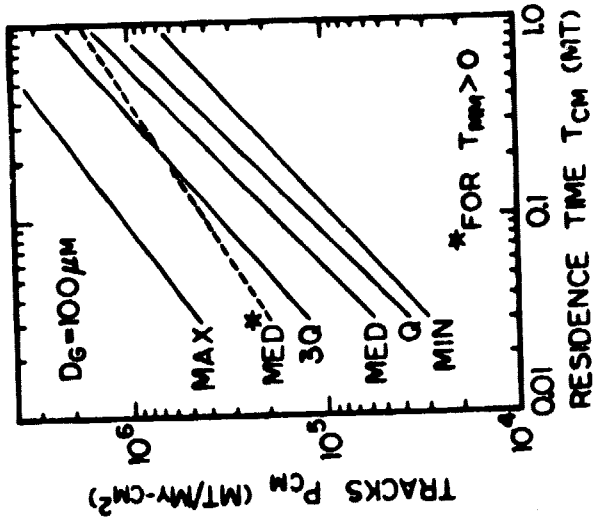

Fig 7

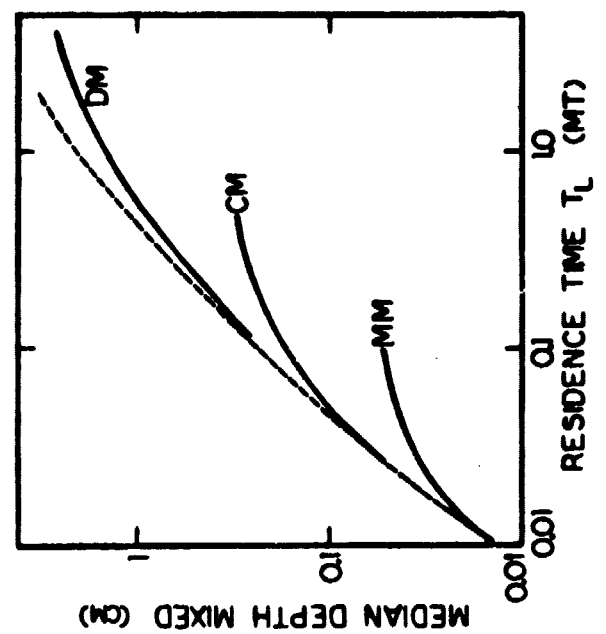

Fig 10

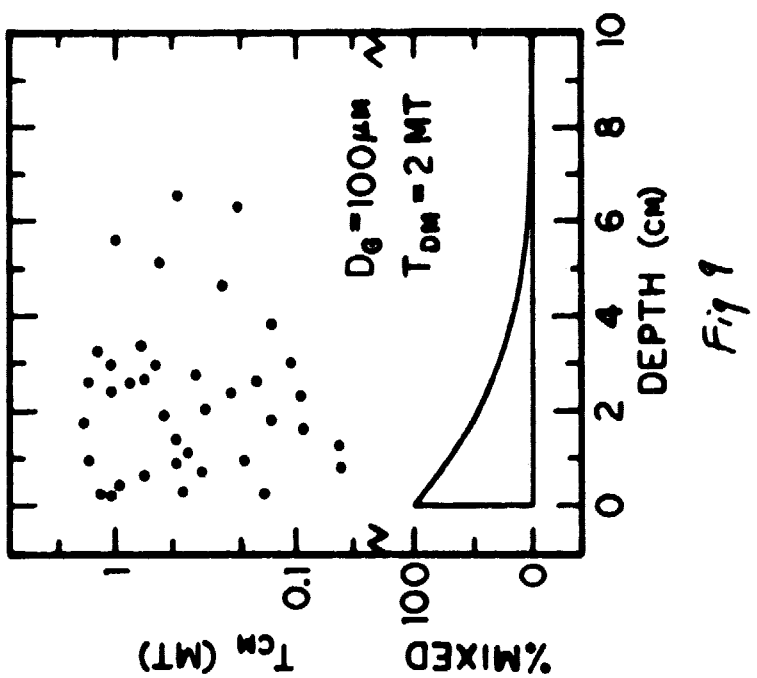

Fig 9

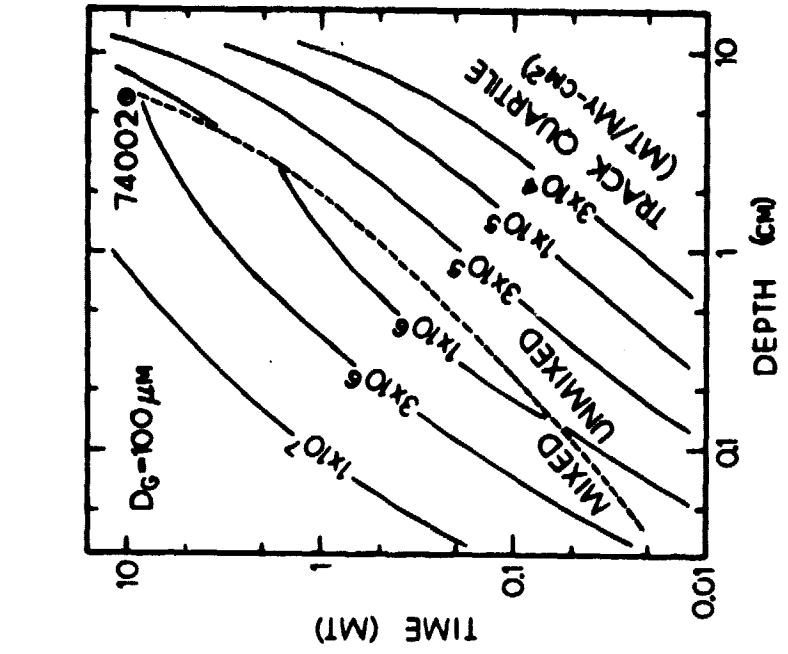

Fig 12

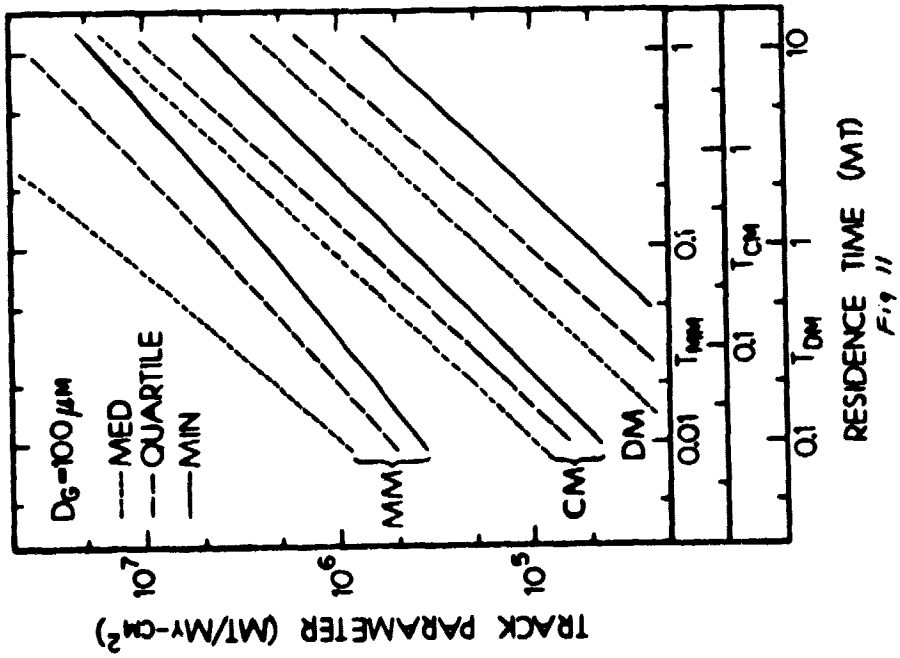

Fig 11

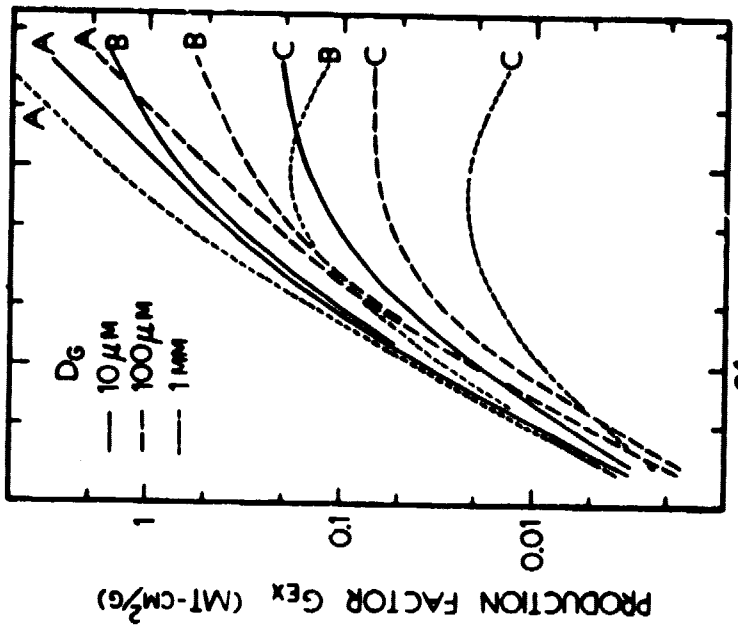

Fig 14

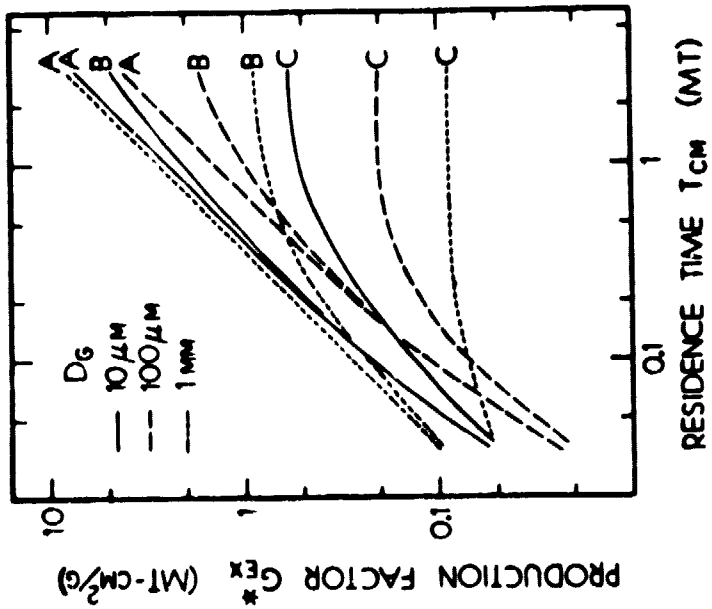

Fig 13

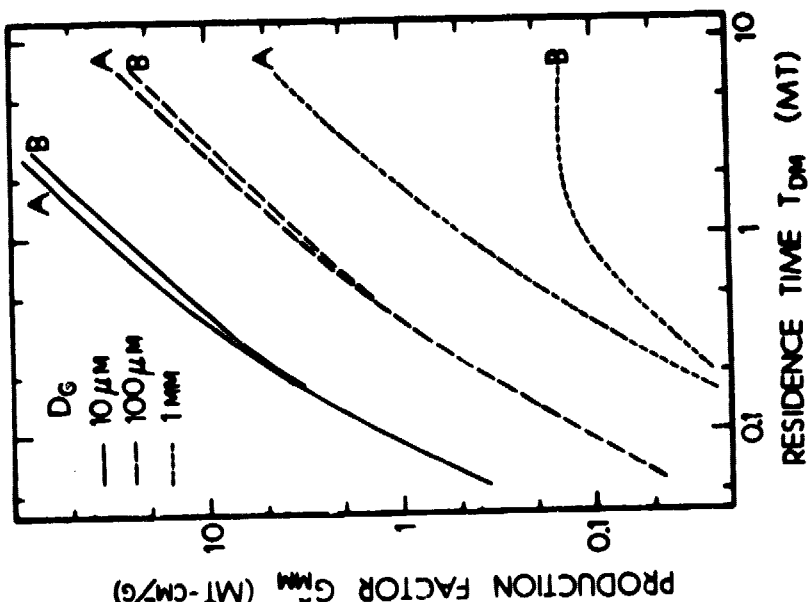

Fig 16

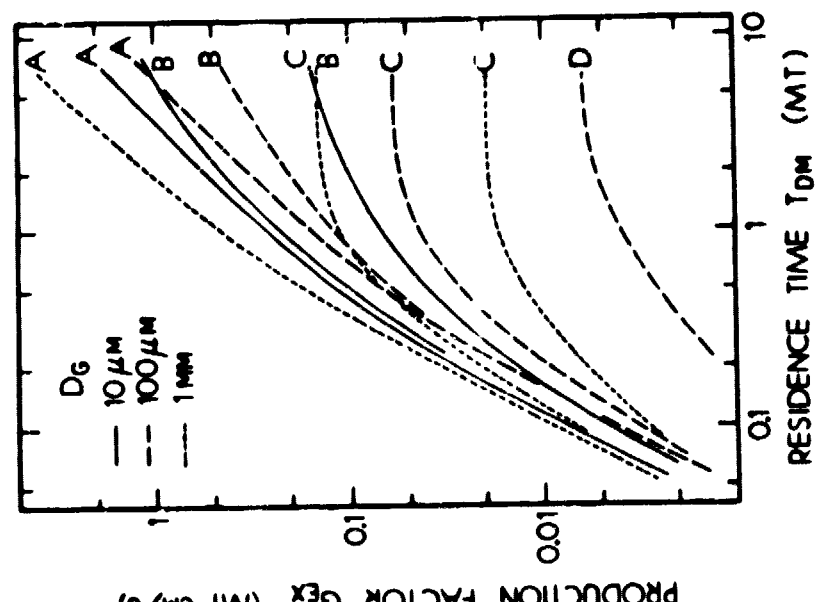

Fig 15

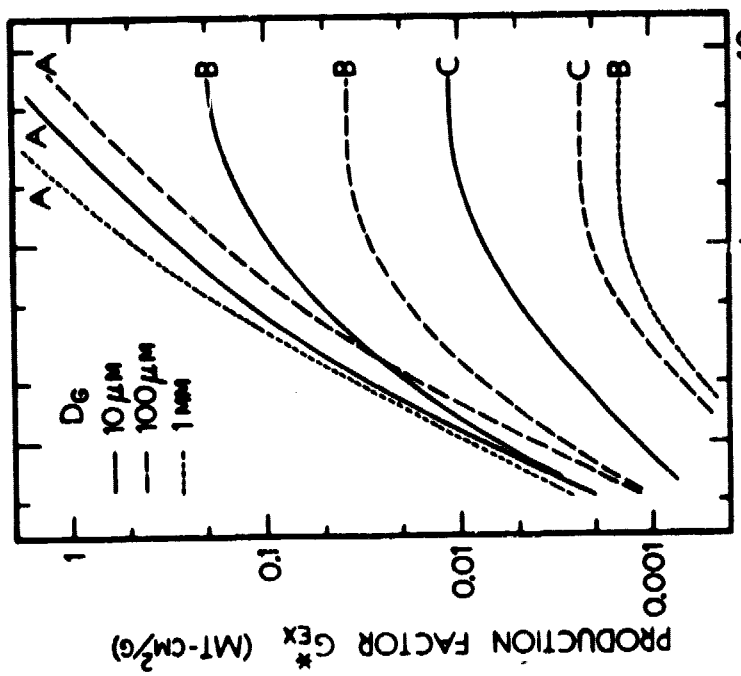

Fig 19

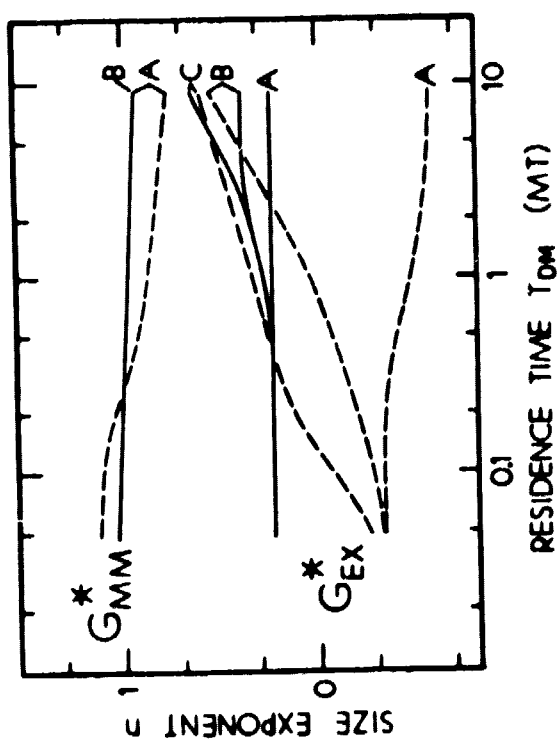

Fig 17